View metadata, citation and similar papers at core.ac.uk
brought to you by CORE
provided by Diposit Digital de la Universitat de Barcelona

1 # NADPH oxidase 4 attenuates cerebral artery changes during the
2 # progression of Marfan syndrome

3

4 Yara Onetti[1], Thayna Meirelles[2], Ana P Dantas[3], Katrin Schröder[4], Elisabet Vila[1],
5 Gustavo Egea[2,3], Francesc Jiménez-Altayó[1]

6

7 [1]Departament de Farmacologia, de Terapèutica i de Toxicologia, Institut de
8 Neurociències, Facultat de Medicina, Universitat Autònoma de Barcelona, Bellaterra,
9 Spain. [2]Departament de Biologia Cel·lular, Immunologia i Neurociències, Facultat de
10 Medicina, Universitat de Barcelona, Barcelona, Spain. [3]Institut Clínic del Tòrax, Institut
11 d'Investigacions Biomèdiques August Pi i Sunyer (IDIBAPS), Barcelona, Spain.
12 [4]Institute for Cardiovascular Physiology, Goethe-University Frankfurt, Frankfurt,
13 Germany.

14

15

16

17 **Correspondence:** Dr F Jiménez-Altayó, Departament de Farmacologia, de
18 Terapèutica i de Toxicologia, Facultat de Medicina, Universitat Autònoma de
19 Barcelona, 08193 Bellaterra (Cerdanyola del Vallès), Spain. E-mail:
20 francesc.jimenez@uab.cat, Tel: (+34) 93 581 1952; Fax: (+34) 93 581 1953

21

22 **Running title:** Nox4 mitigates cerebral artery changes in Marfan syndrome

23

ABSTRACT

Marfan syndrome (MFS) is a connective tissue disorder that is often associated with fibrillin-1 (*Fbn1*) gene mutation and characterized by cardiovascular alterations, predominantly ascending aortic aneurysms. Although neurovascular complications are uncommon in MFS, the improvement in Marfan patients' life expectancy is revealing other secondary alterations, potentially including neurovascular disorders. However, little is known about small vessel pathophysiology in MFS. MFS is associated with hyperactivated transforming growth factor (TGF)-β signaling, which, among numerous other downstream effectors, induces the Nox4 isoform of NADPH oxidase, a strong enzymatic source of H_2O_2. We hypothesized that MFS induces middle cerebral artery (MCA) alterations, and that Nox4 contributes to them. MCA properties from 3-, 6- or 9-month-old Marfan (*Fbn1*$^{C1039G/+}$) mice were compared with those from age/sex-matched wild-type littermates. At 6 months, Marfan compared with wild-type mice developed higher MCA wall/lumen (wild-type: 0.081 ± 0.004; Marfan: 0.093 ± 0.002; 60 mmHg; $P < 0.05$), coupled with increased reactive oxygen species production, TGF-β and Nox4 expression. However, wall stiffness and myogenic autoregulation did not change. To investigate the influence of Nox4 on cerebrovascular properties, we generated Marfan mice with Nox4 deficiency (Nox4$^{-/-}$). Strikingly, Nox4 deletion in Marfan mice aggravated MCA wall thickening (cross-sectional area; Marfan: 6660 ± 363 μm^2; Marfan Nox4$^{-/-}$: 8795 ± 824 μm^2; 60 mmHg; $P < 0.05$), accompanied by decreased TGF-β expression, and increased collagen deposition and Nox1 expression. These findings provide the first evidence that Nox4 mitigates cerebral artery structural changes in a murine model of MFS.

Keywords: fibrillin-1; neurovascular disorders; structural alterations; transforming growth factor-β; Nox4

50 **NEW & NOTEWORTHY**

51 This is the first study to characterize the cerebral artery properties in an animal model
52 of Marfan syndrome. Importantly, we reveal a role for Nox4 in attenuating brain
53 vascular structural changes in Marfan syndrome, which may confer protection against
54 the development of neurovascular disorders during Marfan syndrome progression.

55
56
57
58
59
60
61
62
63
64
65
66
67
68
69
70

71 **INTRODUCTION**

72 Marfan syndrome (MFS) is an autosomal dominant connective tissue disorder with
73 multiple clinical manifestations, including cardiovascular alterations (5, 26). Mutations
74 of the gene encoding fibrillin-1 (*Fbn1*) are the underlying cause (17). Fibrillin-1 is a
75 scaffolding protein that is crucial for elastin deposition and the formation of elastic
76 fibers and laminae (41). Aortic aneurysm leading to aortic dissection and rupture is the
77 event that contributes to premature mortality (5). Neurovascular disorders are
78 uncommon in Marfan patients. In a retrospective hospital-based study, in which
79 patients affected with MFS were seen between 1989 and 1997 (49), no major
80 association of MFS with neurovascular complications has been clearly reported. In
81 addition, the relationship between cerebral artery aneurysms and MFS has been
82 questioned (10, 48, 49). Therefore, the current evidence does not conclusively support
83 a link between MFS and neurovascular disorders. Advances in pharmacological and
84 mainly surgical therapies have resulted in longer life expectancy for Marfan patients
85 (39). However, one consequence of this undoubted improvement could be that Marfan
86 patients are increasingly exposed to other complications, such as those of a
87 neurovascular type. To understand the pathophysiological basis of MFS alterations, a
88 variety of murine experimental models have been developed. The most commonly
89 used is mice heterozygous for the *Fbn1* allele encoding a missense mutation
90 (*Fbn1*$^{C1039G/+}$), which is representative of the most common class of mutation observed
91 in Marfan patients. Marfan mice show impairments in aortic functional and mechanical
92 properties that could contribute to the risk of aortic aneurysm formation (7, 8, 9).
93 However, very little is known about the pathophysiology of small vessels in MFS. To
94 our knowledge, only mesenteric resistance artery properties have been thoroughly
95 analyzed, with reports of Marfan-associated increases in wall stiffness and vasomotor
96 dysfunction (45, 46).

97 Fibrillin-1 form microfibrils, which are a reservoir of transforming growth factor-β (TGF-
98 β) and thus contribute to different aspects of Marfan-related vascular pathophysiology
99 (12, 19, 33). It is well-known that overexpression of TGF-β1 in the brain of non-Marfan
100 animals contributes to cerebrovascular dysfunction (47). On the other hand, vascular
101 NADPH oxidase is a critical source of oxidative stress (20). In this respect, NADPH
102 oxidase 4 (Nox4) is the only family member expressed in the vascular wall (20) whose
103 expression is regulated by TGF-β (6, 13, 22, 38). Nox4 generates H_2O_2 as a reactive
104 oxygen species (ROS), and previous studies have suggested that H_2O_2 regulates
105 arterial structure and function (44). Therefore, we hypothesized that Nox4 could be a
106 relevant downstream effector of TGF-β in the cerebral vasculature in MFS. This
107 hypothesis is based on experimental evidence that shows augmented oxidative stress
108 in aortic and mesenteric artery dysfunction in MFS (46, 50), greater oxidative stress
109 and Nox4 expression in cerebral than in systemic arteries (32), and the relevance of
110 Nox4 as a source of oxidative stress in ischemic stroke (40).

111 Although vascular alterations in systemic arteries have been previously identified in a
112 mouse model of MFS (7, 8, 9, 45, 46, 50), cerebral artery properties have not been
113 investigated. If cerebrovascular abnormalities were present, they might contribute to
114 susceptibility to the development of neurovascular complications. We therefore
115 examined middle cerebral artery (MCA) properties during MFS progression, and
116 subsequently the putative role of Nox4 in the potential alterations that have been
117 observed.

118

119 ## MATERIALS AND METHODS

120 ### Animals

121 Three-, six- and nine-month-old male and female mice were similarly distributed across
122 wild-type (*n* = 26) and *Fbn1*$^{C1039G/+}$ (Marfan; *n* = 25) groups. Marfan mice began with

123 matrices from the Jackson Laboratory (Charles River, Lyon, France). Moreover, 6-
124 month-old wild-type $Nox4^{-/-}$ (*n* = 7) and Marfan $Nox4^{-/-}$ (*n* = 5) mice were used. To
125 establish the Marfan $Nox4^{-/-}$ mice colony, initially wild-type $Nox4^{-/-}$ female mice (42)
126 were bred with *Fbn1*$^{C1039G/+}$ (Marfan $Nox4^{+/+}$) male mice. From the resulting Nox4
127 heterozygous generation ($Nox4^{+/-}$), Marfan male mice were crossed with wild-type
128 female mice to obtain Marfan $Nox4^{-/-}$ male mice that were selected and successively
129 bred with wild-type $Nox4^{-/-}$ female mice. All mice were housed according to institutional
130 guidelines (constant room temperature at 22 °C, 12 h light/dark cycle, 60% humidity,
131 and water ad libitum). All of the experiments were performed under the guidelines
132 established by Spanish legislation (RD 1201/2005) and according to the *Guide for the*
133 *Care and Use of Laboratory Animals,* published by the United States National Institutes
134 of Health (NIH Publications 85-23, revised 1996). Experiments were approved by the
135 *Ethics Committee* of the Universitat de Barcelona, and were carried out in compliance
136 with European legislation.

137

138 **Tissue preparation**

139 MCA from the right and left hemisphere was dissected under a surgical microscope
140 and kept in ice-cold Krebs-Henseleit solution (KHS, composition in mM: NaCl 112.0;
141 KCl 4.7; $CaCl_2$ 2.5; KH_2PO_4 1.1; $MgSO_4$ 1.2; $NaHCO_3$ 25.0; and glucose 11.1) gassed
142 with 95% O_2 and 5% CO_2. The proximal segment of the MCA was immediately used for
143 pressure myography, and at the end of the assay it was handled for nuclei distribution
144 microscopic fluorescence studies (36) and picrosirius red staining (16). Distal MCA
145 segments were used for immunofluorescence (36) and evaluation of superoxide anion
146 production (36). Branches of the MCA and the remaining cerebral arteries were
147 processed for analysis of mRNA levels (36).

148

149 **Pressure myography**

150 Structural, mechanical and myogenic properties of the MCA were studied with a
151 pressure myograph (Danish Myo Tech, model P100; J.P. Trading, Aarhus, Denmark),
152 as described (16, 36). Briefly, vessels were placed on two glass microcannulas and
153 carefully adjusted so that the vessel walls were parallel without stretching them.
154 Intraluminal pressure was then raised to 140 mmHg, and the artery was unbuckled by
155 adjusting the cannulas. Afterwards, the artery was left to equilibrate for 45 min at 40
156 mmHg in gassed KHS (37°C). Intraluminal pressure was reduced to 3 mmHg, and a
157 pressure–diameter curve (3-120 mmHg) was obtained. Internal and external diameters
158 (D_{iCa} and D_{eCa}) were measured for 3 min at each intraluminal pressure. The artery was
159 left to equilibrate for 30 min at 40 mmHg in gassed, calcium-free KHS (37°C; 0 Ca^{2+}:
160 omitting calcium and adding 10 mM EGTA; Sigma-Aldrich, St Louis, MO) and a second
161 pressure-diameter curve (3-120 mmHg) was obtained in passive conditions. Structural,
162 mechanical and myogenic parameters were analyzed as described (16).

163

164 **Nuclei distribution by confocal microscopy**

165 Pressured (40 mmHg)-fixed intact MCA was stained with Hoechst 33342 nuclear dye
166 (10 µg/ml; Sigma-Aldrich) for 30 min (16, 36). Once washing had been completed,
167 arteries were mounted on slides with a well that was made from silicon spacers, to
168 avoid artery deformation. The slides were visualized with a Leica TCS SP2
169 (Heidelberg, Germany) confocal system. Stacks of serial optical slices (0.4 µm thick)
170 were captured from the adventitia to the lumen of each artery. The different MCA layers
171 stained with Hoechst 33342 were clearly distinguished with confocal microscopy,
172 according to the shape and/or orientation of the cell nuclei (1). At least two stacks of
173 images of several regions were captured in each arterial segment. MetaMorph Image

174 Analysis software (Molecular Devices, Sunnyvale, CA) was used for quantification, as
175 reported (16).

176

177 **Elastin determination**

178 Total elastin content was studied in MCA cross-sections (14 μm thick) on the basis of
179 the autofluorescent properties of elastin, as described (35). The fluorescence intensity
180 value was used as an estimate of elastin concentration, following the assumption that
181 the concentration of elastin has a linear relationship with fluorescence intensity (3).
182 Preparations were viewed using a laser scanning confocal microscope (Leica TCS
183 SP2). All the images were taken under identical conditions of zoom (×1), laser
184 intensity, brightness, and contrast. Quantitative analysis of elastin autofluorescence
185 was performed with MetaMorph Image Analysis software (Molecular Devices). The
186 fluorescence signal per area was measured in at least two rings from each animal, and
187 the results were expressed as arbitrary units.

188 The content of elastic fibers in the internal elastic lamina (IEL) was studied in intact
189 pressure (40 mmHg)-fixed MCA using a Leica TCS SP5 confocal microscope. Stacks
190 of serial optical sections (0.3 μm thick) were captured from each artery. At least, two
191 stacks of images of several regions were captured in each arterial segment. All the
192 images were taken under identical conditions of zoom (×5), laser intensity, brightness,
193 and contrast. Quantitative analysis was performed with MetaMorph Image Analysis
194 software (Molecular Devices), as described (24).

195

196 **Collagen determination by picrosirius red staining**

197 MCA sections (14 μm thick) were stained with picrosirius red to determine total
198 collagen (16). Images were taken using a Leica Leitz DMRB microscope equipped with

199 a Leica DC500 camera, and analyzed with MetaMorph Image Analysis software
200 (Molecular Devices). Total collagen content was calculated as a percentage of the
201 stained area of each image obtained under visible light in at least two rings from each
202 animal, and the results were expressed as arbitrary units.

203

204 **Immunofluorescence**

205 Frozen transverse sections (14 μm thick) of MCA were incubated (1 h) with a goat
206 polyclonal antibody against matrix metalloproteinase (MMP)-9 (1:100; R&D Systems,
207 Inc., Minneapolis, MN). After being washed, sections were incubated (45 min) with the
208 secondary antibody (1:200), a donkey anti-goat IgG conjugated to Cyanine 3 (Jackson
209 ImmunoResearch Laboratories, West Grove, PA) at 37°C. The specificity of the
210 immunostaining was verified by omission of the primary antibody, which abolished the
211 fluorescence signal. Quantitative analysis of fluorescence was performed with
212 MetaMorph Image Analysis software (Molecular Devices) and the results were
213 expressed as arbitrary units (36).

214

215 **Measurement of superoxide anion formation**

216 The oxidative fluorescent dye dihydroethidium (DHE) was used to evaluate production
217 of superoxide anion *in situ* (14-μm thick sections) (18). Quantitative analysis of DHE-
218 derived fluorescence was performed with MetaMorph Image Analysis software
219 (Molecular Devices), as reported (16, 36).

220

221 **Quantitative real-time PCR (qRT-PCR)**

222 mRNA expression was quantified by Sybr green-based quantitative real time-PCR as
223 described (34). The expression of mRNA for GAPDH of 18S ribosomal RNA was used
224 as an internal control. qRT-PCR reactions were set up following the manufacturer's
225 guidelines. Ct values obtained for each gene were referenced to GAPDH 18S (ΔΔCt)
226 and converted to the linear form using the term $2^{-\Delta\Delta Ct}$ as a value directly proportional to
227 the copy number of cDNA and the initial quantity of mRNA (34).

228

229 **Statistics**

230 Results are expressed as means ± SE of the number (*n*) of mice indicated in the
231 legends for Figs. 1-6. The difference between wild-type or Marfan mice and the effect
232 of Nox4 deletion was assessed by a two-way ANOVA with Tukey's post-test to
233 compare groups. Data analysis was carried out using GraphPad Prism version 6
234 software. A value of $P < 0.05$ was considered significant.

235

236 **RESULTS**

237 **Structural, mechanical and myogenic properties of MCA during MFS progression**

238 To obtain MCA structural parameters, external and internal diameters were measured
239 under fully relaxed conditions (0 Ca^{2+}-KHS). We did not find a significant difference in
240 external (3 months; wild-type: 167.33 ± 3.41 µm, *n* = 9; Marfan: 169.86 ± 4.23 µm, *n* =
241 7; 6 months; wild-type: 171.00 ± 5.03 µm, *n* = 10; Marfan: 167.18 ± 3.79 µm, *n* = 11; 9
242 months; wild-type: 168.71 ± 6.09 µm, *n* = 7; Marfan: 163.14 ± 2.78 µm, *n* = 7; 60
243 mmHg) or internal (3 months; wild-type: 143.00 ± 2.46 µm, *n* = 9; Marfan: 145.00 ±
244 4.53 µm, *n* = 7; 6 months; wild-type: 146.60 ± 5.20 µm, *n* = 10; Marfan: 141.00 ± 3.25
245 µm, *n* = 11; 9 months; wild-type: 143.43 ± 6.36 µm, *n* = 7; Marfan: 136.00 ± 2.64 µm, *n*
246 = 7; 60 mmHg) diameter in wild-type versus Marfan mice in any age group under study.

247 At 3 months, structural parameters were similar in vessels from control and Marfan
248 mice. However, at 6 months of age, unlike cross-sectional area (Fig. 1*A*) and wall
249 thickness (results not shown), the wall/lumen (Fig. 1*B*) was higher ($P < 0.05$) in Marfan
250 than in wild-type mice, difference that disappeared at 9 months of age. Additionally,
251 neither the cross-sectional area (Fig. 1*A*) nor the wall thickness (results not shown)
252 was modified in Marfan mice at this age.

253 Wall stiffness is a mechanical parameter that can be determined from the stress-strain
254 relationship (2). Since the stress-strain curve is not linear, it is more appropriate to
255 obtain the slope of the curve (β-value). At all mice ages studied, the stress-strain
256 relationship and the β-values were similar, which indicates that MCA stiffness is not
257 altered in Marfan mice (Fig. 2*A*).

258 We did not find a significant difference in internal diameter in active conditions in wild-
259 type versus Marfan mice in any age group under study (3 months; wild-type: 131.11 ±
260 3.41 μm, n = 9; Marfan: 135.14 ± 3.94 μm, n = 7; 6 months; wild-type: 121.00 ± 8.40
261 μm, n = 9; Marfan: 121.70 ± 3.93 μm, n = 10; 9 months; wild-type: 124.86 ± 5.11 μm, n
262 = 7; Marfan: 116.57 ± 4.98 μm, n = 7; 60 mmHg). The analysis of myogenic response
263 as a function of pressure obtained from internal diameter reductions in active relative to
264 passive (0 Ca^{2+}-KHS) conditions revealed that arteries from 3-month-old wild-type mice
265 had less ($P < 0.05$) myogenic tone than arteries of mice from 6 and 9 months (Fig. 2*B*).
266 However, neither the analysis of myogenic response as a function of pressure (Fig. 2*B*)
267 nor the slope of these curves (myogenic reactivity; Table 1) showed significant
268 differences between wild-type and Marfan MCA in all age groups.

269

270 **ROS production in cerebral arteries of Marfan mice and the impact of Nox4**
271 **deletion**

272 We next measured expression levels of the most relevant NADPH oxidases of brain
273 vasculature, as well as ROS production in cerebral arteries from wild-type and Marfan
274 mice (Fig. 3). We evaluated mRNA levels of NADPH oxidase (a major source of
275 vascular superoxide anion) catalytic (Nox1, Nox2, Nox4) and regulatory ($p22^{phox}$)
276 subunits. Marfan cerebral arteries did not show differences in Nox1 and $p22^{phox}$ mRNA
277 expression levels compared with wild-type mice (Fig. 3*A*). In contrast, mRNA levels of
278 Nox4 were significantly higher ($P < 0.05$) in Marfan mice (Fig. 3*A*).

279 To understand the physiological meaning of increased Nox4 expression in MCA of
280 Marfan mice, we generated a Marfan mice model, which was deleted for Nox4 ($Nox4^{-/-}$
281). Taking into account the aforementioned results, we chose animals at six months, in
282 which the most significant vascular changes were observed. Absence of Nox4
283 expression *per se* did not alter either Nox1 or $p22^{phox}$ mRNA levels (Fig. 3*A*). However,
284 Nox4 deficiency in Marfan mice led to higher ($P < 0.05$) Nox1 mRNA expression levels
285 than in wild-type mice (Fig. 3*A*). Unfortunately, Nox2 mRNA levels were undetectable.
286 We also analyzed mRNA levels of Poldip2, which binds to $p22^{phox}$ and enhances Nox4
287 activity (30), and no differences were observed (results not shown). ROS levels were
288 evaluated by DHE-derived fluorescence, and they were higher along the MCA wall of
289 Marfan (two-way ANOVA; $P < 0.01$) mice than in wild-type mice (Fig. 3*B*). However,
290 post-test analysis showed significant increases ($P < 0.05$) in Marfan compared to wild-
291 type mice, but not between Marfan $Nox4^{+/+}$ and Marfan $Nox4^{-/-}$. This suggests that the
292 superoxide anion is not increased via Nox4, but probably through other Nox such as
293 Nox1.

294

295 **TGF-β production in cerebral arteries of Marfan mice and the impact of Nox4**
296 **deletion**

297 We evaluated TGF-β expression in cerebral arteries from wild-type and Marfan mice in
298 the presence and absence of Nox4. Quantitative analysis of TGF-β mRNA levels
299 showed higher (P < 0.05) mRNA expression in Marfan than in wild-type mice (Fig. 4).
300 However, Nox4 deletion attenuated (P < 0.001) TGF-β mRNA expression levels. These
301 results suggest that increases in local TGF-β expression might contribute to
302 augmenting Nox4 expression in the MCA of Marfan mice in a feed-forward fashion.

303

304 **Structural, mechanical and myogenic properties of MCA after Nox4 deletion**

305 We next studied the contribution of Nox4 to the MCA properties of wild-type and
306 Marfan mice (Fig. 5). External (wild-type: 170.40 ± 5.36 μm, n = 5; Marfan: 169.33 ±
307 5.52 μm, n = 6; wild-type Nox4$^{-/-}$: 159.80 ± 4.64 μm, n = 5; Marfan Nox4$^{-/-}$: 178.00 ±
308 4.35 μm, n = 5; 60 mmHg) and internal (wild-type: 146.20 ± 4.74 μm, n = 5; Marfan:
309 142.17 ± 5.12 μm, n = 6; wild-type Nox4$^{-/-}$: 134.60 ± 5.14 μm, n = 5; Marfan Nox4$^{-/-}$:
310 142.80 ± 6.41 μm, n = 5; 60 mmHg) diameters under 0 Ca^{2+}-KHS did not differ in wild-
311 type Nox4$^{-/-}$ compared with wild-type or Marfan mice. However, external diameters in
312 MCA from Marfan Nox4$^{-/-}$ were more enlarged (P < 0.01) than in wild-type Nox4$^{-/-}$ mice.
313 It is important to highlight that the absence of Nox4 expression *per se* did not alter the
314 MCA structure. In contrast, deletion of Nox4 in Marfan mice led to an increase (P <
315 0.05) at high intraluminal pressures (from 60 to 120 mmHg) in cross-sectional area
316 (Fig. 5*A*) and wall/lumen (Fig. 5*B*), but not wall thickness (results not shown).
317 Nevertheless, Nox4 deficiency did not alter the wall stiffness (Fig. 5*C*), the internal
318 diameter in active conditions (wild-type: 115.60 ± 9.93 μm, n = 5; Marfan: 113.83 ±
319 3.10 μm, n = 6; wild-type Nox4$^{-/-}$: 120.25 ± 3.90 μm, n = 4; Marfan Nox4$^{-/-}$: 119.20 ±
320 4.55 μm, n = 5; 60 mmHg), the myogenic response as a function of pressure (Fig. 5*D*),
321 and the myogenic reactivity (wild-type: 0.133 ± 0.080, n = 4; Marfan: 0.077 ± 0.063, n =
322 6; wild-type Nox4$^{-/-}$: 0.033 ± 0.062, n = 4; Marfan Nox4$^{-/-}$: 0.007 ± 0.030, n = 5).

323

324 **Distribution of nuclei through the MCA wall**

325 We next examined whether the aforementioned structural differences could be
326 attributed to changes in the cell density of the MCA wall. To this aim, we analyzed the
327 nuclei distribution from intact and pressurized MCA. As reported in Table 2, total wall,
328 adventitial and media MCA volumes, as well as smooth muscle and endothelial cell
329 number, were almost the same in Marfan and wild-type mice. However, the absence of
330 Nox4 in Marfan mice led to an augmented wall volume ($P < 0.01$) and a decrease ($P <$
331 0.05) in adventitial cell number. Taken together, these results suggest that the MCA
332 structural alterations occurring in Marfan mice of 6 months of age would not implicate
333 an increase in the number of wall cell nuclei, regardless of the presence or absence of
334 Nox4.

335

336 **Elastin and collagen contents in the MCA wall**

337 Total elastin fluorescence in MCA cross sections was similar among groups (wild-type:
338 91.8 ± 17.7, *n* = 6; Marfan: 66.8 ± 9.9, *n* = 5; wild-type Nox4$^{-/-}$: 80.8 ± 15.5, *n* = 5;
339 Marfan Nox4$^{-/-}$: 86.8 ± 4.8, *n* = 4). In addition, analysis of internal elastic lamina (IEL)
340 thickness from intact pressurized MCA showed no differences among groups (Table 2).
341 Although values of the average fluorescence intensity per pixel indicated a similar
342 amount of elastin in wild-type and Marfan mice, a reduction ($P < 0.05$) in IEL
343 fluorescence was observed between Marfan Nox4$^{-/-}$ and Marfan Nox4$^{+/+}$mice (Table 2).

344 To investigate whether the observed MCA wall hypertrophy in Marfan mice could be a
345 consequence of excess collagen deposition, we measured the expression and content
346 of collagen and proteins involved in extracellular matrix (ECM) degradation. Neither
347 mRNA levels of collagen 1A1 (Fig. 6*A*) nor collagen deposition along the MCA wall

348 (Fig. 6*B*) was altered in Marfan compared with wild-type mice. However, a Marfan-
349 associated increase ($P < 0.05$) in matrix metalloproteinase (MMP)-9 mRNA levels was
350 observed (Fig. 6*A*). Nox4$^{-/-}$ mice showed an intrinsic increase ($P < 0.05$) of MMP-9
351 mRNA (Fig. 6*A*) that was accompanied by decreased ($P < 0.05$) collagen 1A1 mRNA
352 levels (Fig. 6*A*), with unchanged collagen deposition (Fig. 6*B*). Importantly, Nox4
353 deficiency in Marfan mice led to augmented ($P < 0.05$) collagen deposition (Fig. 6*B*),
354 despite diminished ($P < 0.01$) collagen 1A1 and augmented ($P < 0.01$) MMP-9 mRNA
355 levels (Fig. 6*A*). Protein expression of MMP-9, assessed by immunofluorescence, was
356 higher ($P < 0.05$) in Marfan than in wild-type mice, and was attenuated ($P < 0.05$) by
357 Nox4 deletion (Fig. 6*C*). Overall, these results suggest that collagen degradation is
358 augmented in the MCA of Marfan mice, and that even though transcriptional negative
359 feedback modulation is initiated, net collagen deposition seem to contribute to MCA
360 hypertrophy in Marfan Nox4$^{-/-}$ mice.

361

362 DISCUSSION

363 The aim of the present study was to characterize for the first time the cerebral artery
364 properties of a mouse heterozygous for a mutation in *Fbn1* (*Fbn1*$^{C1039G/+}$), which
365 manifests many clinical features of MFS. We observed that cerebral arteries from
366 Marfan mice, along the progression of the disease (evaluated by the appearance of
367 aortic aneurysm), developed slightly increased wall/lumen, accompanied by unaltered
368 wall stiffness and myogenic autoregulation. At the same time, it is well-known that
369 Marfan mice show hyperactivation of TGF-β signaling (19, 33), which in turn is known
370 that upregulates the expression of Nox4 (6, 13, 22). Consistently, MCA from Marfan
371 mice increased TGF-β and Nox4 mRNA levels. To investigate the potential influence of
372 the Nox4 signaling pathway in cerebral artery properties, we generated Marfan mice
373 with abrogated Nox4 expression. Strikingly, the loss of Nox4 in Marfan mice

374 aggravated structural alterations, which reveals a critical role for Nox4 in preventing
375 cerebrovascular changes in MFS.

376 Large cerebral arteries, like the MCA, contribute substantially to cerebrovascular
377 resistance (21). In this scenario, cerebrovascular adaptations permit brain circulation to
378 maintain cerebral blood flow and meet metabolic demands, despite cardiovascular
379 disturbances (21, 25). In our mouse model of MFS, MCA wall/lumen was increased at
380 6 months of age, which suggests age-related (i.e. not pre-existing) minor cerebral
381 artery structural alterations in MFS. The increase in wall/lumen is a known adaptive
382 process that contributes to maintaining cerebrovascular resistance and protecting
383 downstream microcirculation from elevated arterial blood pressure, which can
384 subsequently lead to vascular dysfunction (2). However, we did not observe significant
385 wall/lumen differences in 9-month-old mice, most likely due to the slight age-dependent
386 decline of this parameter in wild-type mice. Remarkably, Marfan animals did not display
387 significant alterations in MCA wall stiffness during aging. In contrast, both aorta (8) and
388 mesenteric arteries (46) from Marfan mice showed enhanced wall stiffness. In addition,
389 the lack of changes in middle cerebral artery myogenic tone and reactivity suggest that
390 myogenic autoregulatory mechanisms are preserved. Taken together, the different
391 magnitude of changes observed during MFS progression in systemic (7, 8, 9, 45, 46,
392 50) compared to cerebral arteries suggests region-specific differences in sensitivity to
393 MFS, and highlights that cerebral blood flow is tightly regulated.

394 Increased ROS production and/or oxidative stress have been found to be involved in
395 systemic artery alterations related to MFS (46, 50). Accordingly, we observe that, MCA
396 from Marfan mice also showed augmented ROS generation when compared to wild-
397 type. Even though ROS production is often linked to an increase in vascular collagen
398 deposition (4), we did not detect significant collagen accumulation in MCA from 6-
399 month-old Marfan mice. ECM breakdown mediated by MMP has been associated with
400 thoracic aortic aneurysm in MFS (8). Here, we have found augmented MMP-9 protein

401 expression in the MCA of Marfan mice, which could explain the increase in collagen
402 degradation. In addition, although fibrillin-1 is a scaffolding protein that is crucial for
403 elastin assembly (41), fibrillin-1 defects in Marfan animals do not seem to be coupled
404 with an apparent disruption of MCA wall elastin. Collectively, the absence of major
405 Marfan-induced ECM alterations in MCA are in contrast with changes reported in aorta
406 (8, 12, 14), but support previous findings that challenge the supposed association
407 between MFS and cerebral artery aneurysms (10, 48, 49). Nevertheless, we have to be
408 cautious in generalizing these results to human beings, as our study is limited to one of
409 the various available experimental murine models of MFS, whose clinical symptoms
410 are highly variable depending on their penetrance.

411 Unlike wild-type mice, Marfan $Nox4^{-/-}$ compared with Marfan $Nox4^{+/+}$ mice presented
412 greater MCA collagen deposition, which is a sign of fibrosis and vascular damage,
413 despite showing a transcriptional negative feedback loop involving decreased collagen
414 1A1 and increased MMP-9. Augmentation of collagen deposition probably contributes
415 to increased MCA cross-sectional area in Marfan $Nox4^{-/-}$ mice, which was not
416 associated with alterations in wall stiffness. These data support previous findings that
417 changes in the quantity, distribution and organization of new collagen are determinant
418 to defining the stiffness of the arterial wall (4).

419 Recent studies report an inverse relationship between vascular H_2O_2 production and
420 collagen deposition (31, 44, 51). Nox4 is an important source of oxidative stress in
421 cerebral arteries (32) that seems to play a pathophysiological role in the brain (40).
422 However, unlike Nox1 and Nox2, Nox4 also exerts a protective role in the vasculature
423 (20, 27, 42). This difference could be due to Nox4 capacity to produce H_2O_2, which is
424 the main detectable ROS that is produced, rather than the superoxide anion (43). It has
425 been suggested that Poldip2-mediated, and possibly, Nox4-derived H_2O_2 production
426 could reduce aortic collagen deposition (30, 44). Consistent with this idea, studies
427 show convincing evidence that MMP-9 activation and expression is positively

428 modulated by H_2O_2 predisposing to aortic aneurysm formation (37). In our study, the
429 presence of Nox4 was associated with increased MMP-9 protein expression in the
430 MCA of Marfan mice. Besides, significant collagen deposition was only observed after
431 Nox4 deletion in Marfan mice. However, based on present data we cannot confirm
432 whether Nox4-derived H_2O_2 might repress MCA collagen deposition in MFS. In
433 addition, upregulation of aortic Nox1 can promote superoxide anion production and
434 collagen formation (15). Thus, we cannot exclude the possibility that a Nox4-dependent
435 negative modulatory effect on Nox1-derived superoxide anion production might also
436 contribute to mitigating collagen accumulation in the MCA of Marfan mice.

437 Current evidence has not established a clear link between MFS and neurovascular
438 disorders (10, 48, 49), but since life expectancy increases in MFS patients who have
439 been diagnosed and treated, they could be exposed to more potential causes of
440 neurovascular disorders. The present study is the first to report the development of
441 modest but potentially relevant cerebrovascular alterations in an experimental murine
442 model of MFS. This study also contributes to our understanding of the role of the TGF-
443 β/Nox4 signaling pathway in cerebral vasculature in healthy, and particularly in Marfan
444 patients, since we show that genetic deletion of Nox4 in Marfan mice induces collagen
445 deposition which contributes to arterial wall hypertrophy, thereby causing overt MCA
446 structural alterations. In fact, previous evidence suggests a pathophysiological role of
447 Nox4 in brain damage (40). Overall, the results of the present study suggest that Nox4
448 has a role in regulating cerebrovascular resistance in Marfan animals. Thus, our
449 findings lead to the hypothesis that an overall reduction in TGF-β signaling, an ongoing
450 therapeutic approach against aortic aneurysm formation in MFS (29), might have a
451 negative impact on brain circulation. Similarly, recent evidence supports a critical role
452 of TGF-β signaling in maintaining postnatal aortic homeostasis (23, 28), and an early
453 protective role of TGF-β during aortic aneurysm progression (11). However, further

454 evidence is required to corroborate that Nox4 activation could actually play a beneficial
455 role in the cerebral circulation of Marfan patients.

456

457 **ACKNOWLEDGMENTS**

458 We are grateful to Federica Dinolfo and Vanessa Hernandez for their excellent
459 technical assistance, to Dr. Darya Gorbenko Del Blanco for helpful comments, and to
460 the confocal microscopy core from the Universitat Autònoma de Barcelona.

461

462 **GRANTS**

463 The research was funded by Ministerio de Ciencia e Innovación (SAF2010-19282;
464 SAF2014-56111-R) grants to E.V., a Generalitat de Catalunya (2014SGR574) grant to
465 E.V. and F.J-A., and grants from the Ministerio de Ciencia e Innovación (BFU23012-
466 33932), the Fundación Ramon Areces (Areces11-07) and the Generalitat de Catalunya
467 (2014SGR334) to G.E. G.E. also acknowledges the National Marfan Foundation for its
468 support. Additionally, this work was supported by a Deutsche Forschungsgemeinschaft
469 (DFG; SFB815/TP1) grant to K.S. Y.O. is a predoctoral fellow (FPU) of the Ministerio
470 de Educación y Ciencia (Spain) and T.M. was supported by a fellowship from the
471 National Council of Technological and Scientific Development - Science without
472 Borders scholarship program (Brazilian Federal Government)

473

474 **DISCLOSURES**

475 No conflicts of interest, financial or otherwise, are declared by the author(s).

476

477 **REFERENCES**

478 1. Arribas SM, Hillier C, González C, McGrory S, Dominiczak AF, McGrath JC.
479 Cellular aspects of vascular remodeling in hypertension revealed by confocal
480 microscopy. *Hypertension* 30: 1455-1464, 1997.

481 2. Baumbach GL, Heistad DD. Remodeling of cerebral arterioles in chronic
482 hypertension. *Hypertension* 13: 968-972, 1989.

483 3. Blomfield J, Farrar JF. The fluorescent properties of maturing arterial elastin.
484 *Cardiovasc Res* 3: 161-170, 1969.

485 4. Briones AM, Arribas SM, Salaices M. Role of extracellular matrix in vascular
486 remodeling of hypertension. *Curr Opin Nephrol Hypertens* 19: 187-194, 2010.

487 5. Canadas V, Vilacosta I, Bruna I, Fuster V. Marfan syndrome. Part 1:
488 pathophysiology and diagnosis. *Nat Rev Cardiol* 7: 256-265, 2010.

489 6. Carmona-Cuenca I, Roncero C, Sancho P, Caja L, Fausto N, Fernández M,
490 Fabregat I. Upregulation of the NADPH oxidase NOX4 by TGF-beta in
491 hepatocytes is required for its pro-apoptotic activity. *J Hepatol* 49: 965-976,
492 2008.

493 7. Chung AW, Au Yeung K, Cortes SF, Sandor GG, Judge DP, Dietz HC, van
494 Breemen C. Endothelial dysfunction and compromised eNOS/Akt signaling in
495 the thoracic aorta during the progression of Marfan syndrome. *Br J Pharmacol*
496 150: 1075-1083, 2007a.

497 8. Chung AW, Au Yeung K, Sandor GG, Judge DP, Dietz HC, van Breemen C.
498 Loss of elastic fiber integrity and reduction of vascular smooth muscle
499 contraction resulting from the upregulated activities of matrix metalloproteinase-

500 2 and -9 in the thoracic aortic aneurysm in Marfan syndrome. *Circ Res* 101:
501 512-522, 2007b.

502 9. Chung AW, Yang HH, van Breemen C. Imbalanced synthesis of
503 cyclooxygenase-derived thromboxane A2 and prostacyclin compromises
504 vasomotor function of the thoracic aorta in Marfan syndrome. *Br J Pharmacol*
505 152: 305-312, 2007c.

506 10. Conway JE, Hutchins GM, Tamargo RJ. Marfan syndrome is not asso- ciated
507 with intracranial aneurysms. *Stroke* 30:1632-1636, 1999.

508 11. Cook JR, Clayton NP, Carta L, Galatioto J, Chiu E, Smaldone S, Nelson CA,
509 Cheng SH, Wentworth BM, Ramirez F. Dimorphic effects of transforming
510 growth factor-β signaling during aortic aneurysm progression in mice suggest a
511 combinatorial therapy for Marfan syndrome. *Arterioscler Thromb Vasc Biol* 35:
512 911-917, 2015.

513 12. Crosas-Molist E, Meirelles T, López-Luque J, Serra-Peinado C, Selva J, Caja L,
514 Del Blanco DG, Uriarte JJ, Bertran E, Mendizábal Y, Hernández V, García-
515 Calero C, Busnadiego O, Condom E, Toral D, Castellà M, Forteza A, Navajas
516 D, Sarri E, Rodríguez-Pascual F, Dietz HD, Fabregat I, Egea G. Vascular
517 Smooth Muscle Cell Phenotypic Changes in Patients With Marfan Syndrome.
518 *Arterioscler Thromb Vasc Biol* 35: 960-972, 2015.

519 13. Cucoranu I, Clempus R, Dikalova A, Phelan PJ, Ariyan S, Dikalov S, Sorescu
520 D. NADPH oxidase 4 mediates transforming growth factor-beta1-induced
521 differentiation of cardiac fibroblasts into myofibroblasts. *Circ Res* 97: 900-907,
522 2005.

523 14. Cui JZ, Tehrani AY, Jett KA, Bernatchez P, van Breemen C, Esfandiarei M.
524 Quantification of aortic and cutaneous elastin and collagen morphology in
525 Marfan syndrome by multiphoton microscopy. *J Struct Biol* 187: 242-253, 2014.

526 15. Dammanahalli JK, Wang X, Sun Z. Genetic interleukin-10 deficiency causes
527 vascular remodeling via the upregulation of Nox1. *J Hypertens* 29: 2116-2125,
528 2011.

529 16. Dantas AP, Onetti Y, Oliveira MA, Carvalho MH, Heras M, Vila E, Jiménez-
530 Altayó F. Western diet consumption promotes vascular remodeling in non-
531 senescent mice consistent with accelerated senescence, but does not modify
532 vascular morphology in senescent ones. *Exp Gerontol* 55: 1-11, 2014.

533 17. Dietz HC, Cutting CR, Pyeritz RE, Maslen CL, Sakai LY, Corson GM,
534 Puffenberger EG, Hamosh A, Nanthakumar EJ, Curristin SM, Stetten G,
535 Meyers DA, Francomano CA. Marfan syndrome caused by a recurrent de novo
536 missense mutation in the fibrillin gene. *Nature* 352: 337-339, 1991.

537 18. Dikalov S, Griendling KK, Harrison DG. Measurement of reactive oxygen
538 species in cardiovascular studies. *Hypertension* 49: 717-727, 2007.

539 19. Doyle JJ, Gerber EE, Dietz HC. Matrix-dependent perturbation of TGFβ
540 signaling and disease. *FEBS Lett* 586: 2003-2015, 2012.

541 20. Drummond GR, Sobey CG. Endothelial NADPH oxidases: which NOX to target
542 in vascular disease? *Trends Endocrinol Metab* 25:452-463, 2014.

543 21. Faraci FM, Heistad DD. Regulation of large cerebral arteries and cerebral
544 microvascular pressure. *Circ Res* 66: 8-17, 1990.

545 22. Hecker L, Vittal R, Jones T, Jagirdar R, Luckhardt TR, Horowitz JC, Pennathur
546 S, Martinez FJ, Thannickal VJ. NADPH oxidase-4 mediates myofibroblast

547 activation and fibrogenic responses to lung injury. *Nat Med* 15: 1077-1081,
548 2009.

549 23. Hu JH, Wei H, Jaffe M, Airhart N, Du L, Angelov SN, Yan J, Allen JK, Kang I,
550 Wight TN, Fox K, Smith A, Enstrom R, Dichek DA. Postnatal Deletion of the
551 Type II Transforming Growth Factor-β Receptor in Smooth Muscle Cells
552 Causes Severe Aortopathy in Mice. *Arterioscler Thromb Vasc Biol* 35: 2647-
553 2656, 2015.

554 24. Jiménez-Altayó F, Martín A, Rojas S, Justicia C, Briones AM, Giraldo J, Planas
555 AM, Vila E. Transient middle cerebral artery occlusion causes different
556 structural, mechanical, and myogenic alterations in normotensive and
557 hypertensive rats. *Am J Physiol Heart Circ Physiol* 293: H628-H635, 2007.

558 25. Johnson AC, Cipolla MJ. The cerebral circulation during pregnancy: adapting to
559 preserve normalcy. *Physiology (Bethesda)* 30: 139-147, 2015.

560 26. Judge DP, Dietz HC. Marfan's syndrome. *Lancet* 366: 1965-1976, 2005.

561 27. Konior A, Schramm A, Czesnikiewicz-Guzik M, Guzik TJ. NADPH oxidases in
562 vascular pathology. *Antioxid Redox Signal* 20: 2794-2814, 2014.

563 28. Li W, Li Q, Jiao Y, Qin L, Ali R, Zhou J, Ferruzzi J, Kim RW, Geirsson A, Dietz
564 HC, Offermanns S, Humphrey JD, Tellides G. Tgfbr2 disruption in postnatal
565 smooth muscle impairs aortic wall homeostasis. *J Clin Invest* 124: 755-767,
566 2014.

567 29. Loeys BL. Angiotensin receptor blockers: a panacea for Marfan syndrome and
568 related disorders? Drug Discov Today. 20: 262-266, 2015.

569 30. Lyle AN, Deshpande NN, Taniyama Y, Seidel-Rogol B, Pounkova L, Du P,
570 Papaharalambus C, Lassègue B, Griendling KK. Poldip2, a novel regulator of

571 Nox4 and cytoskeletal integrity in vascular smooth muscle cells. *Circ Res* 105:
572 249-259, 2009.

573 31. Maiellaro-Rafferty K, Weiss D, Joseph G, Wan W, Gleason RL, Taylor WR.
574 Catalase overexpression in aortic smooth muscle prevents pathological
575 mechanical changes underlying abdominal aortic aneurysm formation. *Am J*
576 *Physiol Heart Circ Physiol* 301: H355-H362, 2011.

577 32. Miller AA, Drummond GR, Schmidt HH, Sobey CG. NADPH oxidase activity and
578 function are profoundly greater in cerebral versus systemic arteries. *Circ Res*
579 97: 1055-1062, 2005.

580 33. Neptune ER, Frischmeyer PA, Arking DE, Myers L, Bunton TE, Gayraud B,
581 Ramirez F, Sakai LY, Dietz HC. Dysregulation of TGF-beta activation
582 contributes to pathogenesis in Marfan syndrome. *Nat Genet* 33: 407-411, 2003.

583 34. Novensa L, Selent J, Pastor M, Sandberg K, Heras M, Dantas AP. Equine
584 estrogens impair nitric oxide production and endothelial nitric oxide synthase
585 transcription in human endothelial cells compared with the natural 17{beta}-
586 estradiol. *Hypertension* 56: 405-411, 2010.

587 35. Ogalla E, Claro C, Alvarez de Sotomayor M, Herrera MD, Rodriguez-Rodriguez
588 R. Structural, mechanical and myogenic properties of small mesenteric arteries
589 from ApoE KO mice: characterization and effects of virgin olive oil diets.
590 *Atherosclerosis* 238: 55-63, 2015.

591 36. Onetti Y, Dantas AP, Pérez B, Cugota R, Chamorro A, Planas AM, Vila E,
592 Jiménez-Altayó F. Middle cerebral artery remodeling following transient brain
593 ischemia is linked to early postischemic hyperemia: a target of uric acid
594 treatment. *Am J Physiol Heart Circ Physiol* 308: H862-H874, 2015.

595 37. Parastatidis I, Weiss D, Joseph G, Taylor WR. Overexpression of catalase in
596 vascular smooth muscle cells prevents the formation of abdominal aortic
597 aneurysms. *Arterioscler Thromb Vasc Biol* 33: 2389-2396, 2013.

598 38. Peshavariya HM, Chan EC, Liu GS, Jiang F, Dusting GJ. Transforming growth
599 factor-β1 requires NADPH oxidase 4 for angiogenesis in vitro and in vivo. *J Cell*
600 *Mol Med* 18: 1172-1183, 2014.

601 39. Pyeritz RE, Loeys B. The 8th international research symposium on the Marfan
602 syndrome and related conditions. *Am J Med Genet A* 158: 42-49, 2012.

603 40. Radermacher KA, Wingler K, Langhauser F, Altenhöfer S, Kleikers P, Hermans
604 JJ, Hrabě de Angelis M, Kleinschnitz C, Schmidt HH. Neuroprotection after
605 stroke by targeting NOX4 as a source of oxidative stress. *Antioxid Redox Signal*
606 18: 1418-1427, 2013.

607 41. Reinhardt DP, Chalberg SC, Sakai LY. The structure and function of fibrillin.
608 *Ciba Found Symp* 192: 128-143, 1995.

609 42. Schroder K, Zhang M, Benkhoff S, Mieth A, Pliquett R, Kosowski J, Kruse C,
610 Luedike P, Michaelis UR, Weissmann N, Dimmeler S, Shah AM, and Brandes
611 RP. Nox4 is a protective reactive oxygen species generating vascular NADPH
612 oxidase. *Circ Res* 110: 1217-1225, 2012.

613 43. Serrander L, Cartier L, Bedard K, Banfi B, Lardy B, Plastre O, Sienkiewicz A,
614 Fórró L, Schlegel W, Krause KH. NOX4 activity is determined by mRNA levels
615 and reveals a unique pattern of ROS generation. *Biochem J* 406: 105-114,
616 2007.

617 44. Sutliff RL, Hilenski LL, Amanso AM, Parastatidis I, Dikalova AE, Hansen L,
618 Datla SR, Long JS, El-Ali AM, Joseph G, Gleason RL Jr, Taylor WR, Hart CM,
619 Griendling KK, Lassègue B. Polymerase delta interacting protein 2 sustains

620 vascular structure and function. *Arterioscler Thromb Vasc Biol* 33: 2154-2161,
621 2013.

622 45. Syyong HT, Chung AW, van Breemen C. Marfan syndrome decreases Ca2+
623 wave frequency and vasoconstriction in murine mesenteric resistance arteries
624 without changing underlying mechanisms. *J Vasc Res* 48: 150-162, 2011.

625 46. Syyong HT, Chung AW, Yang HH, van Breemen C. Dysfunction of endothelial
626 and smooth muscle cells in small arteries of a mouse model of Marfan
627 syndrome. *Br J Pharmacol* 158: 1597-1608, 2009.

628 47. Tong XK, Nicolakakis N, Kocharyan A, Hamel E. Vascular remodeling versus
629 amyloid beta-induced oxidative stress in the cerebrovascular dysfunctions
630 associated with Alzheimer's disease. *J Neurosci* 25: 11165-11174, 2005.

631 48. van den Berg JS, Limburg M, Hennekam RC. Is Marfan syndrome associated
632 with symptomatic intracranial aneurysms? *Stroke* 27:10-12, 1996.

633 49. Wityk RJ, Zanferrari C, Oppenheimer S. Neurovascular complications of marfan
634 syndrome: a retrospective, hospital-based study. *Stroke* 33: 680-684, 2002.

635 50. Yang HH, van Breemen C, Chung AW. Vasomotor dysfunction in the thoracic
636 aorta of Marfan syndrome is associated with accumulation of oxidative stress.
637 *Vascul Pharmacol* 52: 37-45, 2010.

638 51. Zhou RH, Vendrov AE, Tchivilev I, Niu XL, Molnar KC, Rojas M, Carter JD,
639 Tong H, Stouffer GA, Madamanchi NR, Runge MS. Mitochondrial oxidative
640 stress in aortic stiffening with age: the role of smooth muscle cell function.
641 *Arterioscler Thromb Vasc Biol* 32: 745-755, 2012.

642

643

644 **FIGURE CAPTIONS**

645 **Fig. 1.** Structural properties of middle cerebral arteries in 3-, 6- and 9-month-old wild-
646 type and Marfan mice. (A) Cross-sectional area (CSA)-intraluminal pressure in passive
647 conditions (0 Ca^{2+}-KHS) and (B) wall/lumen-intraluminal pressure. Results are the
648 means ± SE from wild-type (3 months: *n* = 9; 6 months: *n* = 9; 9 months: *n* = 7) and
649 Marfan (3 months: *n* = 7; 6 months: *n* = 11; 9 months: *n* = 7) mice. *$P < 0.05$ by two-
650 way ANOVA.

651 **Fig. 2.** Mechanical and myogenic properties of middle cerebral arteries in 3-, 6-, 9-
652 month-old wild-type and Marfan mice. (A) Stress-Strain (D_i/D_o). (B) Internal diameter in
653 active (2.5 mM Ca^{2+}-KHS; D_{iCa}) relative to passive (D_{i0Ca}) conditions. D_o, internal
654 diameter at 3 mmHg; D_i, observed internal diameter from a given intravascular
655 pressure. Results are the means ± SE from wild-type (3 months: *n* = 9; 6 months: *n* =
656 7-8; 9 months: *n* = 7) and Marfan (3 months: *n* = 7; 6 months: *n* = 7-11; 9 months: *n* =
657 6-7) mice.

658 **Fig. 3.** Influence of Nox4 deletion ($Nox4^{-/-}$) on reactive oxygen species production of
659 middle cerebral arteries in 6-month-old wild-type and Marfan mice. (A) Comparative
660 analysis of cerebral artery mRNA levels of the NADPH oxidase subunit Nox1, Nox4
661 and $p22^{phox}$. mRNA levels are expressed as $2^{-\Delta\Delta Ct}$ using 18S as internal control. (B)
662 Representative photomicrographs and quantitative analysis of fluorescence intensity of
663 confocal microscopic middle cerebral artery sections labelled with the oxidative dye
664 dihydroethidium (DHE), which produces a red fluorescence when oxidized by
665 superoxide anion. END, endothelium; SM, smooth muscle; ADV, adventitia. Results
666 are the means ± SE from wild-type (*n* = 5), Marfan (*n* = 5), wild-type $Nox4^{-/-}$ (*n* = 5-7)
667 and Marfan $Nox4^{-/-}$ (*n* = 5) mice. *$P < 0.05$, **$P < 0.01$, ***$P < 0.001$ by two-way
668 ANOVA with Tukey's post-test. All experimental groups were compared against each
669 other but only significant comparisons are indicated.

670 **Fig. 4.** Influence of Nox4 deletion ($Nox4^{-/-}$) on transforming growth factor (TGF)-β
671 mRNA levels of cerebral arteries in 6-month-old wild-type and Marfan mice. mRNA
672 levels are expressed as $2^{-\Delta\Delta Ct}$ using 18S as internal control. Results are the means ±
673 SE from wild-type (*n* = 5), Marfan (*n* = 5), wild-type $Nox4^{-/-}$ (*n* = 7) and Marfan $Nox4^{-/-}$ (*n*
674 = 5) mice. *$P < 0.05$, ***$P < 0.001$ by two-way ANOVA with Tukey's post-test. All
675 experimental groups were compared against each other but only significant
676 comparisons are indicated.

677 **Fig. 5.** Influence of Nox4 deletion ($Nox4^{-/-}$) on structural, mechanical and myogenic
678 properties of middle cerebral arteries in 6-month-old wild-type and Marfan mice. (A)
679 Cross-sectional area (CSA)-intraluminal pressure in passive conditions (0 Ca^{2+}-KHS).
680 (B) wall/lumen-intraluminal pressure. (C) Stress-Strain (D_i/D_o). (D) Internal diameter in
681 active (2.5 mM Ca^{2+}-KHS; D_{iCa}) relative to passive (D_{i0Ca}) conditions. D_o, internal
682 diameter at 3 mmHg; D_i, observed internal diameter from a given intravascular
683 pressure. Results are the means ± SE from wild-type (*n* = 5), Marfan (*n* = 6), wild-type
684 $Nox4^{-/-}$ (*n* = 5) and Marfan $Nox4^{-/-}$ (*n* = 5) mice. *$P < 0.05$ by two-way ANOVA. All
685 experimental groups were compared against each other but only significant
686 comparisons are indicated.

687 **Fig. 6.** Influence of Nox4 deletion ($Nox4^{-/-}$) on collagen expression and homeostasis of
688 middle cerebral arteries in 6-month-old wild-type and Marfan mice. (A) Comparative
689 analysis of cerebral artery mRNA levels of collagen 1A1 (Col1A1) and matrix
690 metalloproteinase (MMP)-9. mRNA levels are expressed as $2^{-\Delta\Delta Ct}$ using 18S as internal
691 control. (B) Representative photomicrographs and quantitative analysis of total middle
692 cerebral artery collagen staining using picrosirius red. (C) Representative
693 photomicrographs and quantification of MMP-9 immunofluorescence of confocal
694 microscopic middle cerebral artery sections. Results are the means ± SE from wild-
695 type (*n* = 5-7), Marfan (*n* = 5), wild-type $Nox4^{-/-}$ (*n* = 4-5) and Marfan $Nox4^{-/-}$ (*n* = 5)
696 mice. *$P < 0.05$; **$P < 0.01$ by two-way ANOVA with Tukey's post-test. All experimental

697 groups were compared against each other but only significant comparisons are
698 indicated.

699

700

Table 1 Slope value (myogenic reactivity) of the myogenic response as a function of pressure curve in middle cerebral arteries from 3-, 6- and 9-month-old wild-type and Marfan mice.

	wild-type	**Marfan**
Age (months)		
3	0.062 ± 0.033	0.043 ± 0.033
6	0.095 ± 0.038	0.108 ± 0.061
9	0.104 ± 0.049	0.064 ± 0.027

Results are the means ± SE from wild-type (3 months: n = 9; 6 months: n = 7; 9 months: n = 7) and Marfan (3 months: n = 7; 6 months: n = 7; 9 months: n = 7) mice.

Table 2 Comparison of nuclei distribution and internal elastic lamina elastin content in pressurized segments of middle cerebral arteries from 6-month-old wild-type and Marfan mice in the presence and absence of Nox4.

	Nox4$^{+/+}$		**Nox4$^{-/-}$**	
	wild-type	**Marfan**	**wild-type**	**Marfan**
Wall volume (mm^3)	0.006 ± 0.0004	0.007 ± 0.0002	0.006 ± 0.0002	0.008 ± 0.0008**
Adventitial volume (mm^3)	0.004 ± 0.0004	0.004 ± 0.0008	0.004 ± 0.0005	0.004 ± 0.0015
Media volume (mm^3)	0.002 ± 0.0007	0.002 ± 0.0006	0.002 ± 0.0006	0.002 ± 0.0007
Number of AC/mm^3	144 ± 105	399 ± 96	158 ± 102	34 ± 21*
Number of SMC/mm^3	1279 ± 129	1131 ± 118	1115 ± 177	1302 ± 232
Total number of EC	781 ± 71	553 ± 133	745 ± 138	897 ± 66
IEL thickness (μm)	2.9 ± 0.4	3.0 ± 0.4	3.4 ± 0.6	2.6 ± 0.2
IEL fluorescence intensity (average pixel)	23.6 ± 6.5	28.6 ± 3.8	22.3 ± 3.5	13.5 ± 2.0*

AC, adventitial cells; SMC, smooth muscle cells; EC, endothelial cells; IEL, internal elastic lamina. Results are the means ± SE from wild-type (*n* = 5), Marfan (*n* = 5), wild-type Nox4$^{-/-}$ (*n* = 5) and Marfan Nox4$^{-/-}$ (*n* = 5) mice. * $P < 0.05$, ** $P < 0.01$, Marfan vs. Marfan Nox4$^{-/-}$ by two-way ANOVA with Tukey's post-test.

Fig. 1

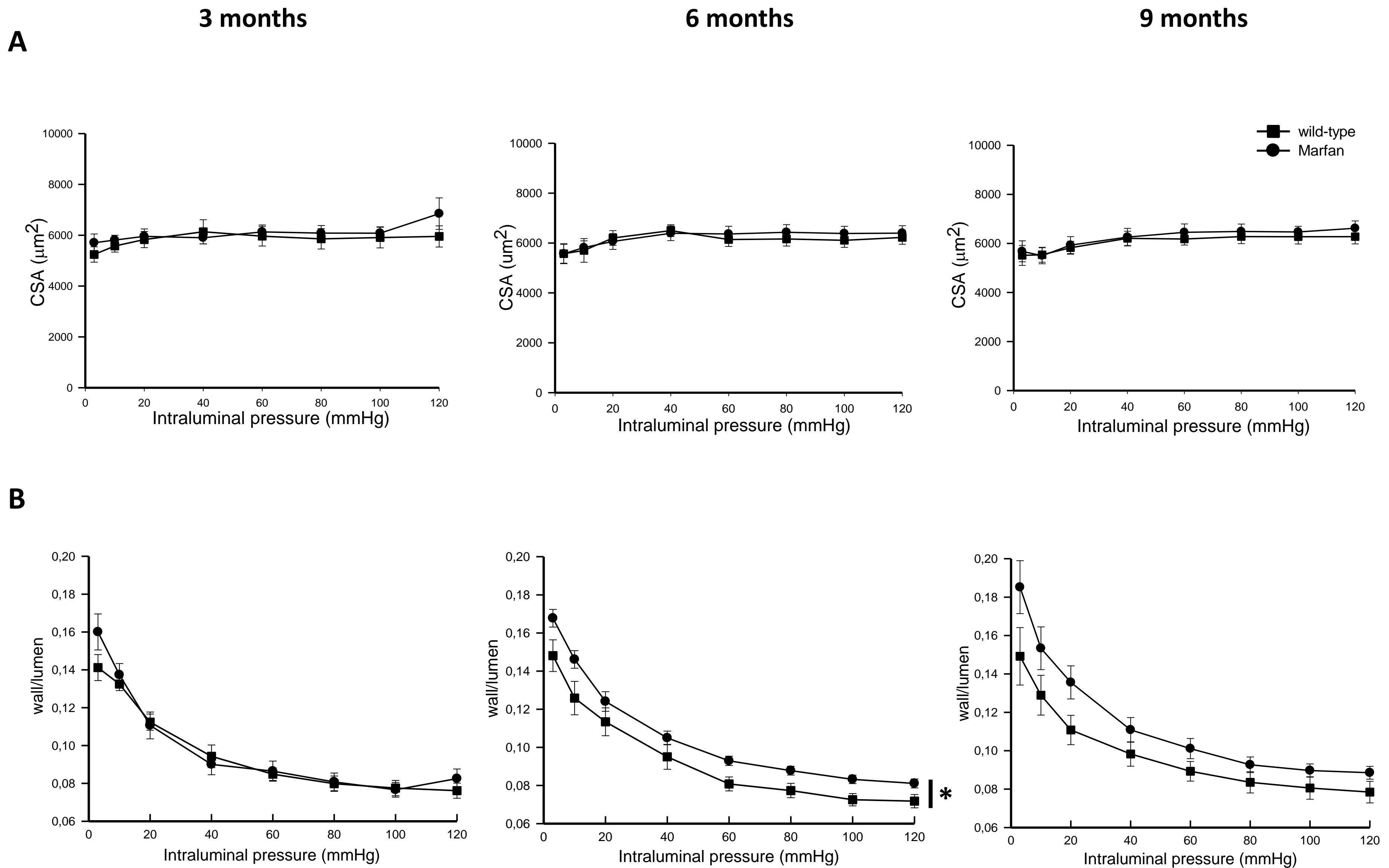

Fig. 2

A

3 months **6 months** **9 months**

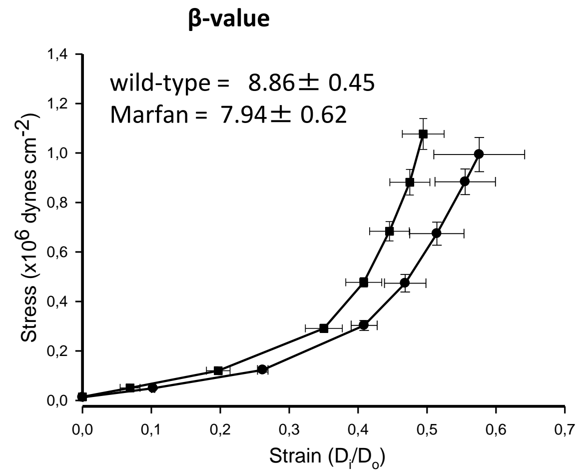

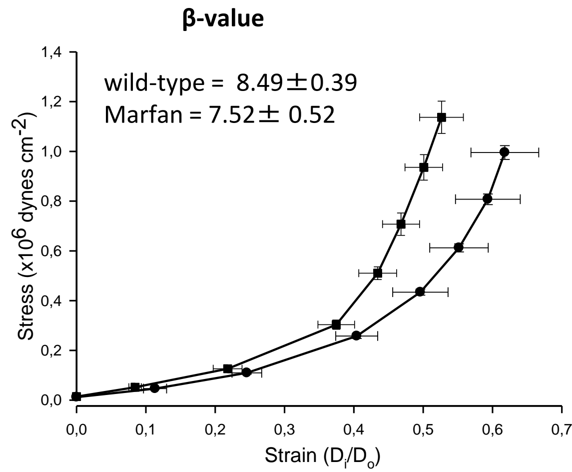

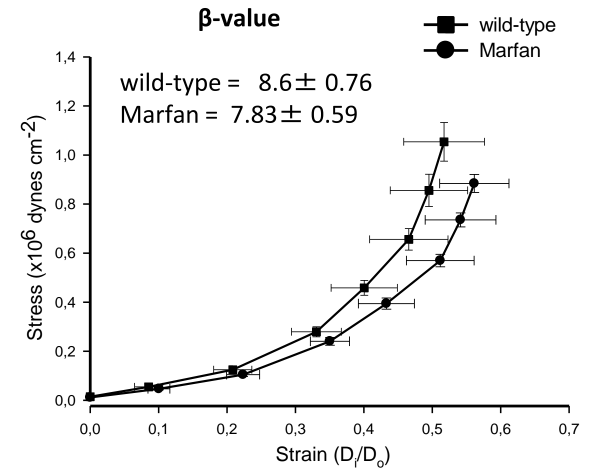

B

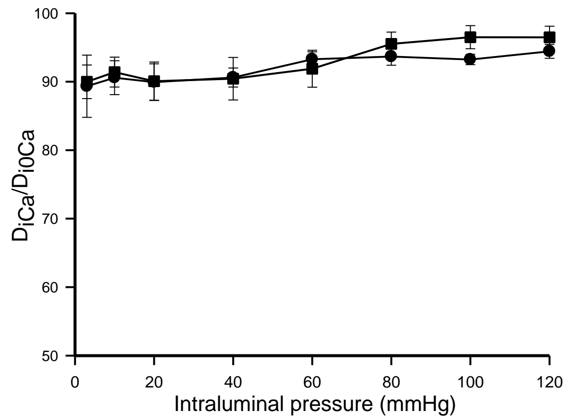

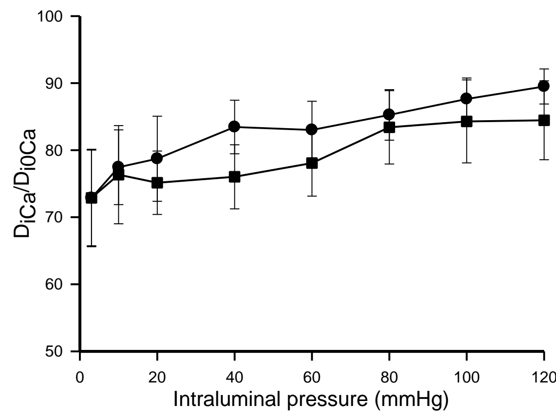

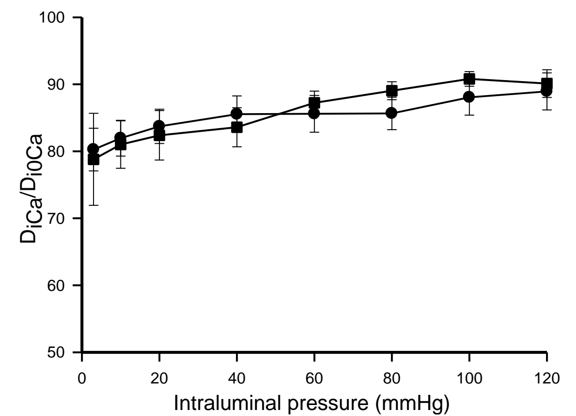

Fig. 3

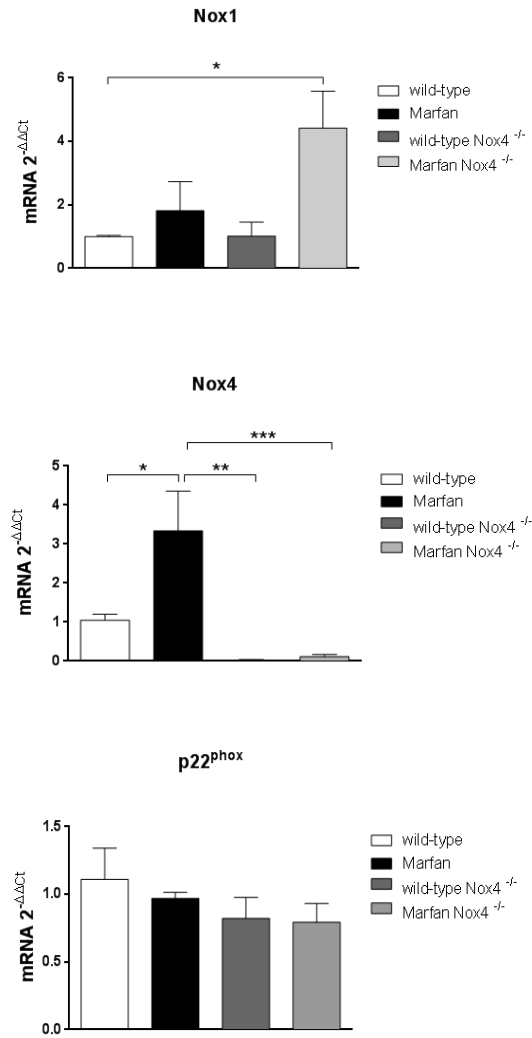

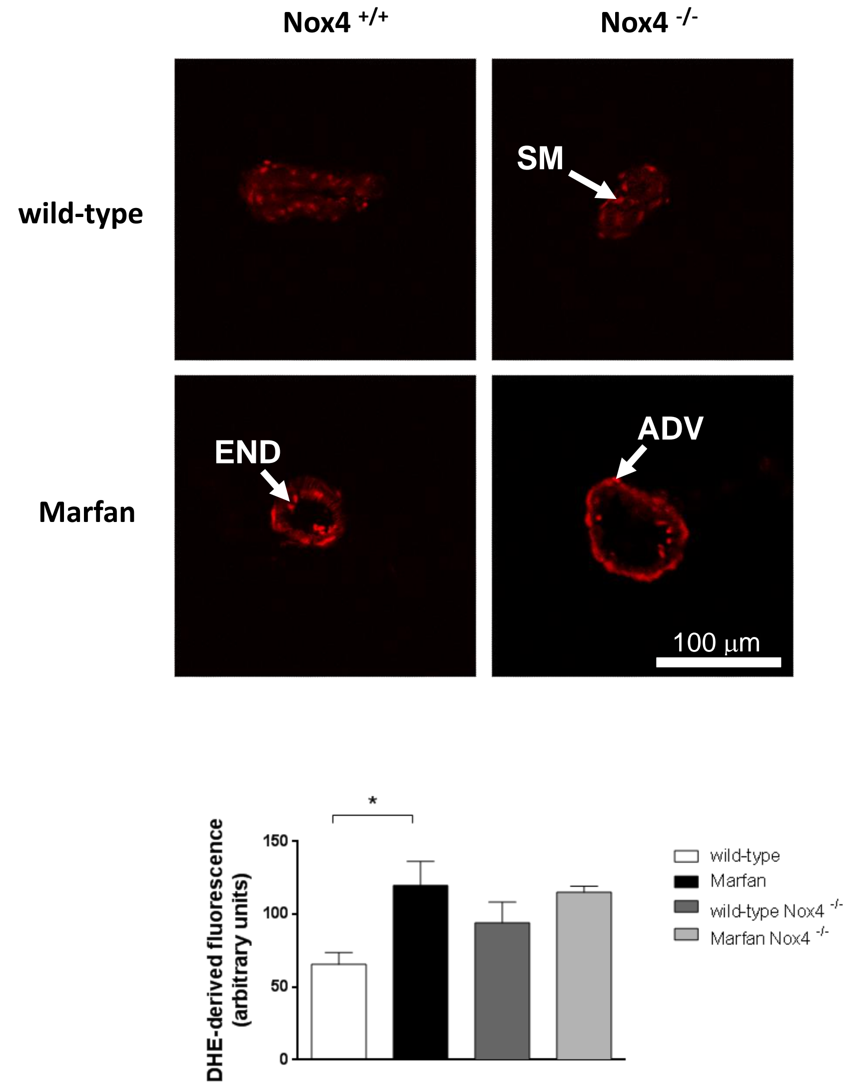

Fig. 4

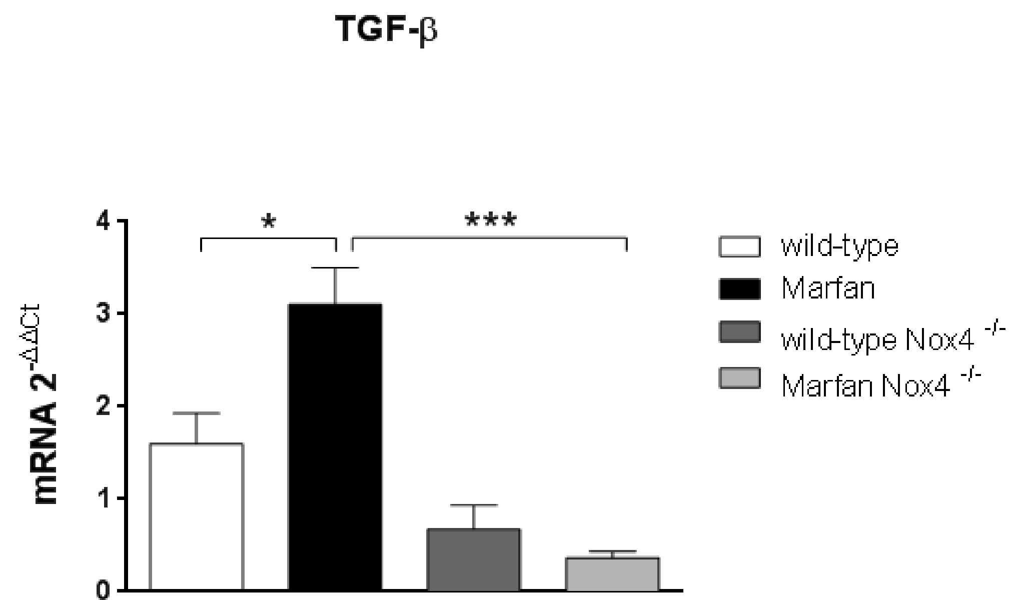

Fig. 5

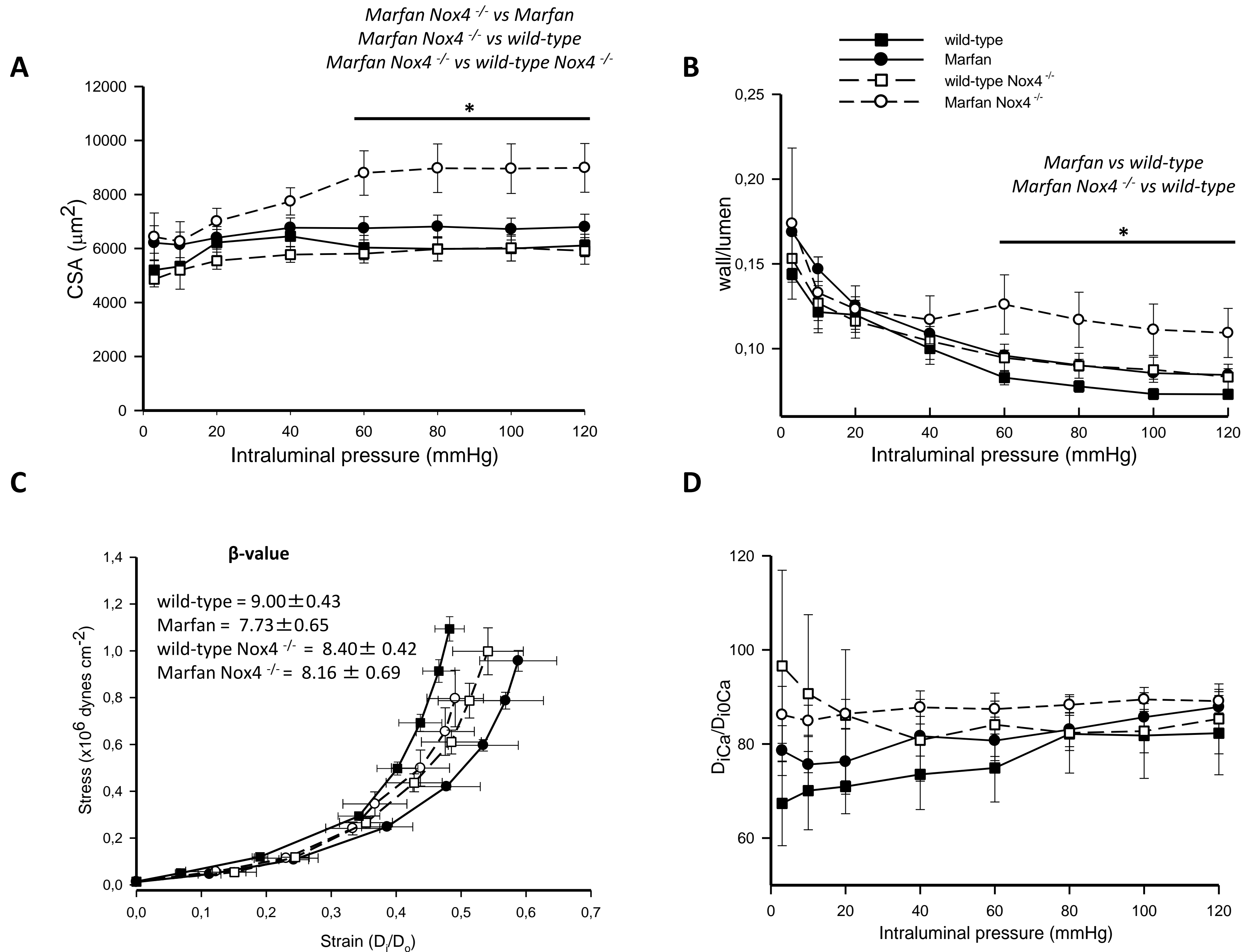

Fig. 6

A

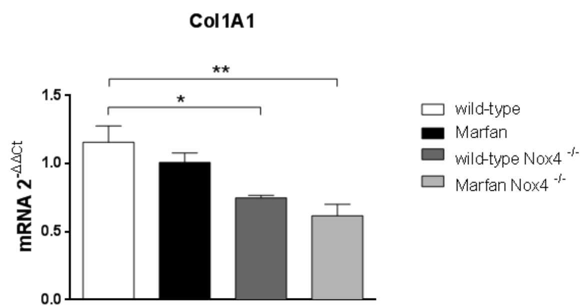

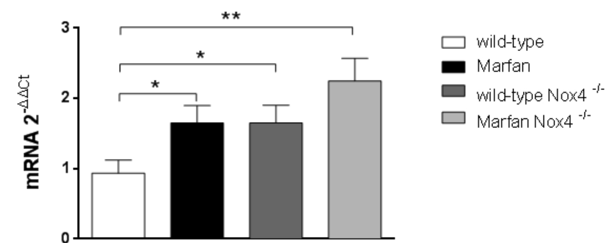

B

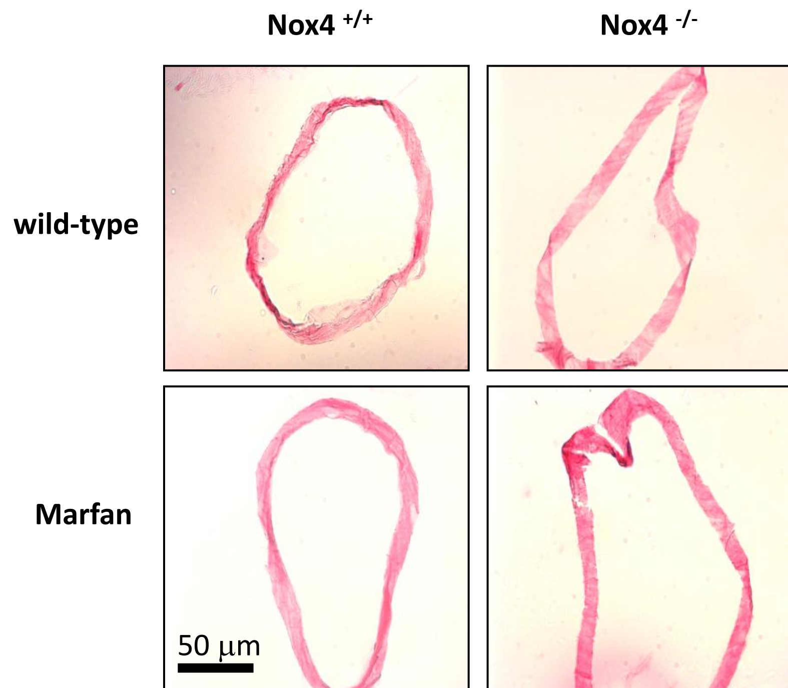

C